Experimental study of backflow air leakage through an opening from a depressurized enclosure

Zeinab Rida, Salima Kaissoun, Corinne Prevost, Thomas Gelain, Eric Climent

Experimental study of backflow air leakage through an opening from a depressurized enclosure.

Zeinab Rida[1,2*], Salima Kaissoun[1,2] , Corinne Prevost[1], Thomas Gelain[1] and Eric Climent[2]

[1] *Institut de Radioprotection et de Sûreté Nucléaire (IRSN), PSN-RES, SCA, Gif sur Yvette, 91192, France;* [2] *Institut de Mécanique des Fluides de Toulouse (IMFT) - CNRS, Université de Toulouse, 31400 Toulouse, France*

In the nuclear decommissioning and dismantling operations, a dynamic confinement is applied to all openings in order to prevent the transfer of pollutants outside depressurized enclosures and to insure the safety of workers. To guaranty an efficient dynamic confinement, ISO 16647 and ISO 17873 standards recommend to maintain a constant value for the inward flow velocity near the opening depending on the level of radioactive pollution hazard. The main purpose of this work is to identify the possible conditions under which flow inversions near the opening may lead to gaseous pollutant leakage and then failure of the dynamic confinement. We aim at quantifying the amount of this pollutant backflow. The leakage from an experimental ventilated enclosure with a small opening on its frontal wall has been investigated. Laser flow visualizations and Particle Image Velocimetry (PIV) measurements showed that the presence of an additional turbulent jet flow in competition with the inward confinement flow is among the main causes leading to the leakage through the opening. The gas tracing technique has provided experimental data to quantify the pollutant backflow and allowed to compare the different scenarios. We conclude that a new criterion based on local aeraulic conditions near the opening is

relevant to guaranty an efficient confinement.

Keywords: Dynamic confinement; Flow inversion; Turbulent jet; Backflow pollutants

*Corresponding author. Email: zeinab.rida@irsn.fr

1. Introduction

Operations of decommissioning and maintenance in nuclear facilities require ventilated enclosures around contaminated equipment in order to prevent the leakage of radioactive materials towards the atmospheric environment. These enclosures are operated with a negative pressure relative to the room where they are installed. By means of extraction systems, air is sucked through openings that can be either inherent to the design of the enclosure or accidental, and generates directional airflow ensuring the dynamic confinement of hazardous material. However, due to some operating works and fluctuating differential pressure on both sides of the opening, local and unsteady flow inversions may occur leading to the dispersion of contamination outwards, a phenomenon commonly referred to as backflow. Criteria for the conception of dynamic confinement through nominal or accidental openings in nuclear installations are presented in ISO 16647 standard[2] for decommissioning and maintenance operations and in ISO 17873 standard[1] for laboratories and factories scale. In the past, three values of inlet velocity at the opening were mentioned: 1.5 m/s for the tritium, 1 m/s for the plutonium 238 and 0.5 m/s for any other pollutants. However, the ISO 17873 standard recommends that each case must be investigated specifically, based on the potential risk of contamination, the influence of the aeraulic disturbances,.. ISO 16647 standard indicates the common values of criteria for an efficient confinement such as air direction, air velocity and depression level depending on the potential contamination risk. For example, areas with moderate air contamination potential have to impose an air velocity higher than 1 m/s near a calibrated opening orifice of 100 mm diameter. Areas with very high potential for atmospheric contamination are to be studied on a case-by-case basis. The current study follows the ISO standards recommendations to study each case specifically, and focuses on the evaluation of the relevant criteria to guaranty an efficient dynamic confinement, and then the safety of nuclear operations. To this aim, we need to identify and reproduce the aeraulic scenarios that

may disturb the confinement inflow and possibly lead to backflow of a gaseous pollutant outside the ventilated enclosure through small openings. Then, we can predict and prevent them during operations in maintenance or dismantling sites.

Ventilation systems are employed in many applications to maintain a directional airflow at the openings and thus to limit airborne contaminant dispersion. They are necessary with large-scale openings as large doors for different industrial purposes[3], for building entrances equipped with air curtains[4,5], for refrigerated storage spaces and cold rooms[6,7] and for hospital isolation rooms[8]. They have been also studied in food[9, 10] and electronic industries[11] and for pharmaceutical applications. Tracer gas is used to calculate the dispersion rate in ventilated systems useful for the assessment of control room habitability[21]. Studies confirm that the directional airflow is disturbed by many unsteady events, such as door opening[12, 13], human walking[14] and the presence of temperature gradients[15, 16]. In the context of nuclear safety, many studies have been dedicated to quantifying the intensity and the kinetics of the propagation of polluting agents that result from the breakage of static or dynamic confinement in nuclear ventilated enclosures, for example in the case of fume cupboards or gloves boxes ([17,18]). Tracing gas technique was used to calculate the dispersion rate in ventilated systems useful for the assessment of control room habitability[21]. Simulation method was established in order to predict the tritium behavior after the tritium leak event should happen in ventilated room[22].

Unlike most investigations on the aerodynamic confinement previously described that deal with large openings, the current study is focusing on airflow dynamics through small openings, such as a rectangular slit whose hydraulic diameter does not exceed ten centimeters and where the initial air inflow is fully turbulent. Thanks to preliminary visualization tests, we have observed that the confinement flow directed from the outside towards the

enclosure might be disturbed by an additional parallel or perpendicular flow created inside or outside the enclosure. This flow disturbance causes instabilities in the velocity field near the opening due to its sharp edged geometry and the turbulent nature of flows. To the best of our knowledge, this phenomenon occurring on small rectangular slit was not described yet in the literature because of the large number of possible configurations and the difficulties related to its quantification. In fact, the unsteady and three-dimensional nature of flow structures make it very difficult to observe locally and to capture quantitatively the amount of pollutant released.

In this work, we designed a reduced size ventilated enclosure with a rectangular opening on its frontal wall. A directional inflow is imposed by dynamic confinement, resulting in the three tested inlet velocities at the opening: 0.5 m/s, 1 m/s and 1.5 m/s . A disturbance corresponding to a counter-current turbulent free jet is facing the directional flow produced at the opening, in order to induce the backflow phenomenon as shown in Fig. 1.

The paper is organized as follows. The first part is the description of the experimental setup and the methods used to measure the backflow phenomenon, namely the visualization, the PIV and the gas tracing techniques. The second part focuses on the qualitative results obtained from the visualization and the PIV, and finally we comment on the quantitative results in terms of transfer coefficients. The paper closes with a conclusion and perspectives.

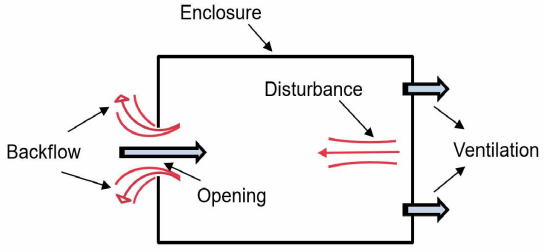

Figure 1 Scheme of the backflow scenario in a ventilated enclosure.

2. Description of experimental setup and measurement techniques

2.1. Experimental enclosure

The geometric characteristics and dimensions of the experimental enclosure have been chosen wisely. First, it should be small in comparison with the airlock workstations and without internal obstacles. Second, it must be adapted to accommodate turbulent jets far from the opening. Thus, an experimental ventilated enclosure chamber of a volume equal to 0.3 m^3 was built, as shown in Fig. 2 (top). It is equipped with an airflow extraction circuit connected to a centrifugal fan.

The experimental model is a sealed and fully transparent PMMA (Plexiglass) enclosure with smooth walls, parallelepipedic shape and internal dimensions of 1.2 m $\times$ 0.5 m $\times$ 0.5 m. The enclosure depth (0.5 m) and width (1.2 m) have been carefully chosen to contain an internal additional turbulent jet located in front of the opening or perpendicular to it, to be in a fully developed regime when reaching the opening.

The enclosure is sketched with its different parts in Fig. 2 (down). The front wall, of (1.06 $\times$ 0.36) m^2 area, is removable, transparent and has a thickness of 5 mm. A rectangular small opening is centered on the enclosure front wall and has a surface of (0.1 $\times$ 0.03) m^2 (the hydraulic diameter is equal to D_h = 46 mm) and a thickness of 5 mm. The rear wall is also removable for a simple access to the enclosure. It supports

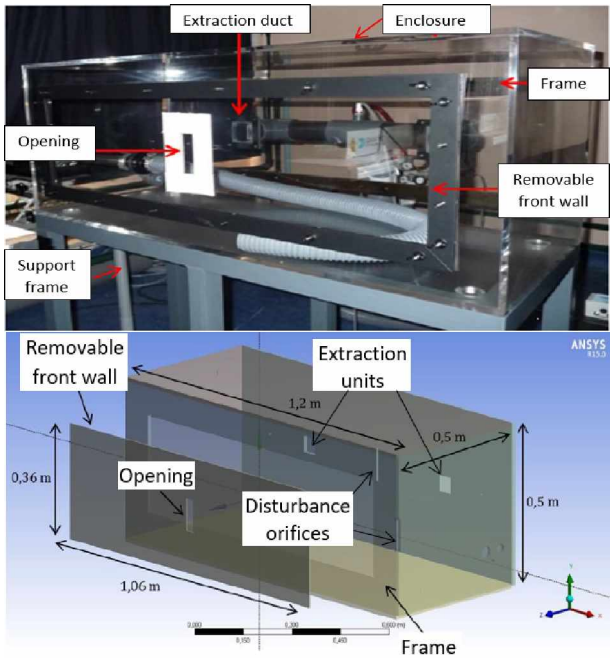

Figure 2 Top: Frontal view of the experimental enclosure showing the opening. Bottom: Sketch of the experimental enclosure with its different parts (CFX scheme).

two identical units of square shape and dimensions $(0.05 \times 0.05)\ m^2$, centered with respect to the median horizontal plane of the enclosure. They are connected to an airflow extraction circuit in order to ensure a homogenous internal pressure field and a directional inflow. The enclosure is depressurized by a centrifugal extraction fan (VSB-14 Plastifer) equipped with a 0 - 50 Hz frequency converter. The extraction rates of the enclosure are fixed depending on the incoming flowrate imposed at the opening (maximum flowrate is of the order of 100 $m^3.h^{-1}$). Nevertheless, we will focus our study on much lower flow rates, of the order of a few cubic meters per hour. The rear wall also contains a rectangular orifice of $(0.1 \times 0.01)\ m^2$ centered with respect to the median horizontal and vertical walls of the enclosure and connected to an injection nozzle in order to produce an internal counter-current turbulent jet injected towards the opening.

Apart from the frontal wall, the enclosure walls have a thickness of 12 mm, which ensures their mechanical resistance in the face of significant depression. Note that all the walls of the enclosure are sealed, except the front and rear walls. The right-hand side wall is

equipped with a circular hole of 8 mm diameter for the tracer gas injection and a circular passage of 40 mm diameter for the extraction of the disturbance. It is also equipped with a rectangular orifice of $(0.1 \times 0.01)\ m^2$ connected to an injection nozzle used in the case of internal parietal disturbing jets. Pressure taps are distributed over the enclosure wall and connected to a probe for the continuous monitoring of the depression inside the enclosure.

2.2. Generation of the flow perturbation

Our study aims to put into interaction two different flows: the flow passing through the opening due to the dynamic confinement of the enclosure, and the aeraulic disturbance originating from a turbulent jet. Three types of aeraulic disturbances have been studied. Due to the enclosure dimensions, they reach the opening in a fully-developed regime.

- The transverse disturbance is a jet flow propagating along the frontal wall and perpendicular to the direction of the inflow entering the opening. It may be located outside the enclosure in the case of an external transverse jet (Fig. 3(a)) or inside the enclosure (injected from the side wall on the right) in the case of the internal transverse jet (Fig. 3(b)).
- The counter-current internal disturbance is a turbulent free jet originating from the rear wall facing the inflow at the opening. The two flows are in opposite direction at the opening (Fig. 3(c)).

Devices producing the internal disturbance are integrated into the system as a closed circuit (shown in red on Fig. 4) in order to keep the enclosure under negative differential pressure.

A centrifugal fan is connected through a duct to the side wall in order to continuously extract part of the flow, which is reinjected into the enclosure through the injection nozzle $(0.1 \times 0.01)\ m^2$ located on the rear wall. A valve is added between the fan and the nozzle in order to vary the disturbance flowrate inside the enclosure. The fan can reach a maximum

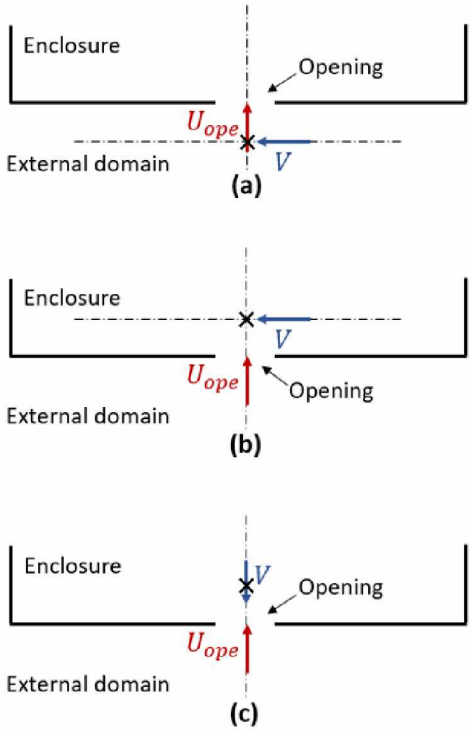

Figure 3 Sketches of the disturbance flow directions in the case of external transverse jet (a), internal transverse jet (b) and internal counter-current jet (c). The symbol "×" in each sketch corresponds to the measurement location of the velocity V.

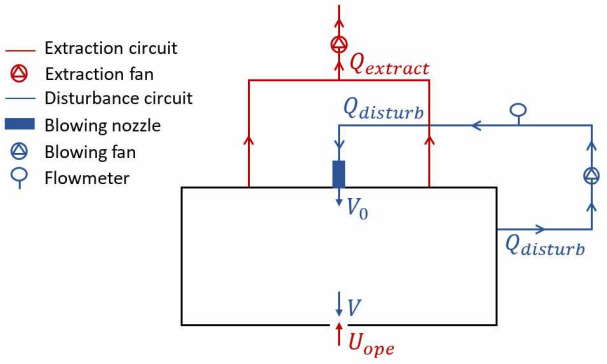

Figure 4 Scheme of the closed circuit of the internal counter-current disturbing jet.

flowrate of about 130 $m^3.h^{-1}$.

2.3. Visualization technique

Visualization methods are applied to observe the flow inversions on both sides of the opening in the presence of a counter-current jet flow. The doubled pulsed laser/CCD camera facility is set in order to, firstly visualize the flow by laser tomography images, and secondly to obtain the velocity fields near the opening from PIV post-processing. The particle image velocimetry (PIV) is a non-intrusive method which consists in capturing two images on two separate frames and performing multistep cross-correlation analysis to obtain the Eulerian velocity fields of the flow[19] on a cartesian grid.

A thin (1-3 mm) light sheet is oriented vertically towards the opening axial plane. Acquisition devices are presented in Fig. 5. The gas phase is seeded with smoke oil particles of 1 micron diameter, as fluid flow tracer particles, produced by SAFEX F2001 Plus particles generator supplied by Dantec Dynamics. The light source is a dual-cavity doubled Nd:YaG pulsed laser emitting at 532 nm, with a maximum energy of 800 mJ per pulse and a maximum frequency of 15 Hz. The image acquisition equipment includes a Flowsense EO 4M digital camera equipped with a CCD sensor of 2048 $\times$ 2048 pixels and an objective of 50 mm (pixel size is 7.4 μm). The camera buffer has a maximum acquisition frequency of 10 Hz and is triggered in synchronization with each pulse of the laser. The control, the synchronization of the laser-camera system and the post-processing of images are carried out using the Dynamic Studio V5 software which provides instantaneous 2D velocity vector fields in the illuminated cross-section of the flow.

2.4. Determination of the backflow factor

In order to quantify the amount of the gaseous pollutant backflow at the opening, a characteristic factor K is defined[20]. It is the ratio between the mean tracer concentration

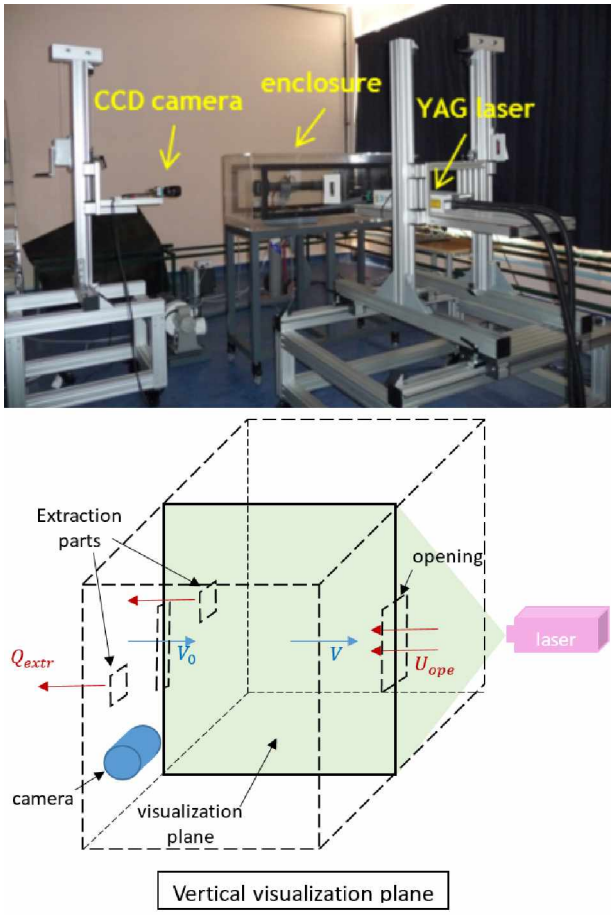

Figure 5 Top: Acquisition devices required for the visualization and PIV measurements. Bottom: Scheme of visualizations and PIV devices in the vertical plane on the enclosure for a counter-current disturbance.

in the air/tracer mixture backflowed locally at the opening outside the enclosure $\overline{C_{out_{eq}}}$ and the tracer concentration in the air/tracer mixture present inside the enclosure $\overline{C_{in_{eq}}}$ at equilibrium (measured at the extraction outlet). This coefficient is expressed as a percentage and is defined by Eq. 1.

$$K = \frac{(\overline{C_{out_{eq}}} - C_{air})}{(\overline{C_{in_{eq}}} - C_{air})} \tag{1}$$

C_{air} is the concentration of the gaseous tracer naturally present in ambient air (5 ± 2 ppm for the case of helium). The concentrations are expressed in volume parts per million (ppm.v). The backflow factor K gives a common reference to the quantity of backflowed pollutant, and consequently allows to compare all tests among each other. The backflow factor K is directly related to the dynamic containment efficiency E by Eq. 2.

$$E = 1 - K \tag{2}$$

We stress that, in nuclear safety, a transfer coefficient k (s/m^3) (Eq. 3) is commonly used to quantify the backflow phenomena that occur during a dynamic containment.

$$k(s/m^3) = \frac{(\overline{C_{out_{eq}}} - C_{air})}{q_0} \tag{3}$$

q_0 is the volume flowrate of the gas tracer injected in the enclosure.

Additionally, we introduce a non-dimensional aeraulic parameter, allowing to characterize the aeraulic conditions at the opening. It is defined as the ratio between the disturbance velocity at the opening V and the local flow of dynamic confinement at the opening U_{ope}: V/U_{ope}. We note that U_{ope} and V are measured independently: U_{ope} is measured when the disturbance flow is stopped and V is measured when the air extraction is

stopped. We will show that, contrary to the criteria used commonly in the ISO standards (minimum velocity at the opening and/or minimum pressure in the enclosure), the dimensionless V/U_{ope} ratio is more appropriate as a relevant parameter to characterize the onset of the pollutant backflow at the opening regardless of the type of aeraulic disturbance. In the following results section, we comment on the evolution of the backflow factor K (%) versus of this dimensionless aeraulic parameter V/U_{ope}.

2.4.1. Determination of the characteristic flow velocities

Determination of the velocity at the opening, U_{ope}

The extraction flowrate applied to the enclosure Q_{ext} and consequently the flow velocity at the opening U_{ope} are determined using the gas tracing technique. It consists of three parts: the injection circuit, the detection device and the acquisition system. The principle is shown schematically in Fig. 6(top). Initially, a constant and controlled tracer gas flow q_0 ($Nl.h^{-1}$) is injected continuously into the enclosure from a compressed pure helium reservoir equipped with a BROOKS 5850E volume flowmeter (0 - 45 $Nl.h^{-1}$). At equilibrium, the concentration $\overline{C_{in_{eq}}}$ of air/tracer is homogenous inside the enclosure and is measured in the extraction circuit as follows. An air/tracer sample is pumped to an Alcatel model ASM 102 mass spectrometer for analysis. A LabVIEW acquisition system insures the continuous monitoring of the helium concentration $\overline{C_{in_{eq}}}$ during the experiment.

The extraction flowrate from the enclosure Q_{ext} is then obtained using tracer mass balance at equilibrium (Eq. 4).

$$Q_{ope}C_{air} + q_0C_0 = Q_{ext}\overline{C_{in_{eq}}} \tag{4}$$

with Q_{ope} is the air flowrate entering through the opening ($m^3.h^{-1}$), q_0 the flowrate of injected gas ($m^3.h^{-1}$), $\overline{C_{in_{eq}}}$ the tracer concentration measured in the system at equilib-

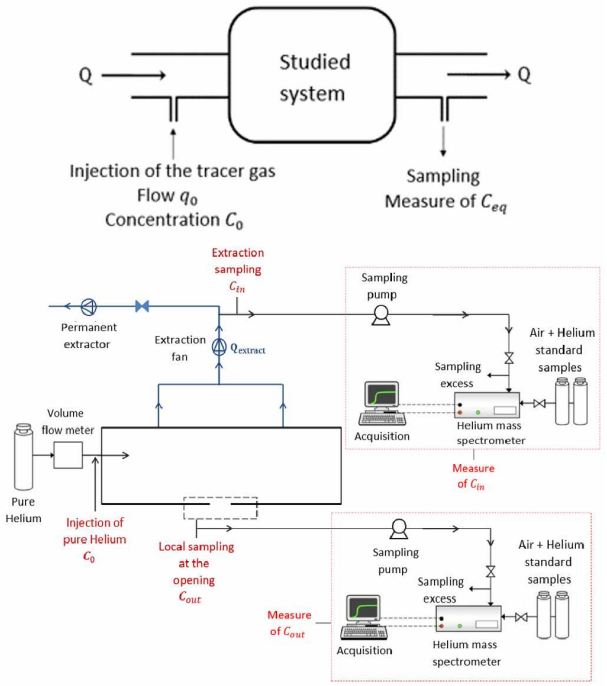

Figure 6 Top: Determination of the airflow through a ventilated system. Bottom: Scheme of the measurement of $\overline{C_{in_{eq}}}$ and $\overline{C_{out_{eq}}}$ using the gas tracing technique.

rium (ppm.v) and Q_{ext} the gas extraction flowrate in the system ($m^3.h^{-1}$). C_{air} is the concentration of the tracer gas naturally present in the air ($C_{air} = 5 \pm 2$ ppm when the tracer gas is helium) and C_0 is the tracer injection concentration (ppm).

Since air admission into the enclosure is only possible through the opening (assuming negligible leaks) and q_0 is negligible compared to Q_{ope} and Q_{ext}, the flow velocity at the opening U_{ope} could be deduced from the extraction flowrate from the enclosure Q_{ext} ($m^3.h^{-1}$) which is obtained from Eq. 5.

$$Q_{ext} = Q_{ope} = U_{ope} \times S \tag{5}$$

where S (m^2) is the surface of the opening.

Determination of the resulting disturbance velocity V at the opening

The aeraulic parameter related to the perturbation flow is the resulting velocity V at the opening. It results from the spatial decay of the turbulent jet velocity of the disturbance along its axis. The latter is measured locally at the opening in the median horizontal plane. The position of the measuring point varies from one disturbance to another (internal/ external wall jet, internal counter-current free jet). For the internal counter-current free jet, the measuring point is inside the enclosure in the plane perpendicular to the frontal wall at 3 cm from the opening. For the case of internal transverse jet, it is located inside the enclosure at the plane parallel to the frontal wall at 3 cm from the opening. For the case of external transverse jet, it is located outside the enclosure in the plane parallel to the frontal wall at 3 cm from the opening. The measurement is carried out using an hot wire sensor of KIMO VT210TF type. The position of the hot wire sensor used for the measurement of the velocity V for each disturbance type is denoted "$\times$" in Fig. 3. Note that these velocities V are measured in absence of the frontal wall of the enclosure for the case of the internal counter-current free jet, and in presence of the frontal wall of the enclosure for the case of the internal and external transverse jets.

2.4.2. Determination of $\overline{C_{in_{eq}}}$ and $\overline{C_{out_{eq}}}$ using the gas tracing technique

The measurement of $\overline{C_{in_{eq}}}$ and $\overline{C_{out_{eq}}}$ is carried out using the gas tracing technique as shown in Fig. 6(down).

Determination of $C_{in_{eq}}$

A first sampling probe is located downstream in the extraction of the enclosure, at a convenient distance to obtain a homogeneous air/helium mixture. A mass spectrometer is added to measure the helium concentration of the air/helium gas mixture in the enclosure. Once equilibrium of the helium concentration is reached in the enclosure and then in the

extraction ducts, the signal remains steady and the average equilibrium value of helium concentration inside the enclosure is noted $\overline{C_{in_{eq}}}$ (ppm). This concentration is measured before the generation of the disturbance.

Determination of $\overline{C_{out_{eq}}}$

The second measurement is an average of many samplers, it records the helium concentration of the air/helium gas mixture backflowed outside the enclosure near the opening, due to the disturbance. The number and the spatial arrangement of samplers located on the periphery of the opening are optimized in order to capture the backflowed gas tracer for each disturbance while preventing to promote the backflow due to their presence. In the case of counter-current perturbation, we added 16 samplers of 3 mm diameter placed on the frontal wall at 3 mm away from the edges of the opening, and 3 samplers uniformly spaced and located in front of the opening at 2.5 cm outside the enclosure, as shown in Fig. 7. In this case, the analysis of the backflowed gas mixture concentration is carried out using an Alcatel model ASM100 mass spectrometer and gives a fluctuating signal. The temporal mean backflowed helium concentration over the samplers is noted $\overline{C_{out_{eq}}}$.

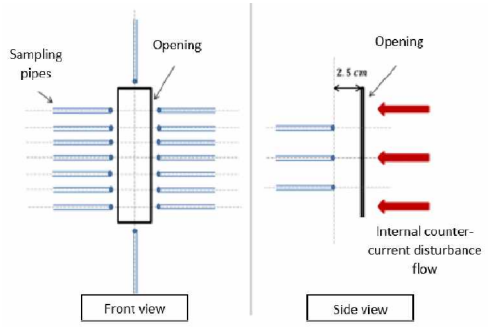

Figure 7 Scheme of the frontal and side views of the samplers positions around the opening.

2.4.3. Estimate of uncertainties

The $U_{r(K)}$ uncertainty is an expanded relative uncertainty, expressed as a percentage, with a coverage factor of 2 corresponding to 95% confidence interval.

The expanded relative uncertainty on the backflow factor K and the ratio V/U_{ope} are given by Eq. 6 and Eq. 7 respectively.

$$U_{r(K)} = \pm 2\sqrt{\left[\frac{U_{r(\Delta C_{in_{eq}})}}{2}\right]^2 + \left[\frac{U_{r(\Delta C_{out_{eq}})}}{2}\right]^2} \tag{6}$$

$$U_{r(V/U_{ope})} = \pm 2\sqrt{\left[\frac{U_{r(U_{ope})}}{2}\right]^2 + \left[\frac{U_{r(V)}}{2}\right]^2} \tag{7}$$

The origins of uncertainties for $\Delta C_{in_{eq}}$ and $\Delta C_{out_{eq}}$ are the temporal drift of the spectrometers between two calibrations, the uncertainty of the instrumentation (spectrometer/acquisition/software unit), the uncertainty associated with the standard mixtures of air/helium bottles and the dispersion of the sampled concentration from the mean value. The uncertainty related to U_{ope} is based on the uncertainty of the injection flowmeter and $\Delta C_{in_{eq}}$. The uncertainty related to V is based on the uncertainty of the hot wire anemometer. Uncertainties will be added to plots with error bars.

3. Observation of leakage and flow measurements

Experiments presented below highlight the competition between the existing air inflow at the opening and the turbulent jet created outside or inside the enclosure, which induces unsteady flow dynamics in the vicinity of the opening. First we present the results obtained for an external transverse jet flow, then those obtained for an internal counter-current jet flow. In both cases, the confinement inflow has been set at the opening to a level corresponding to the velocity $U_{ope} = 1$ m/s (mean extraction flowrate of 10.8 $m^3.h^{-1}$).

Table 1 shows the velocities V_0 at the outlet of the nozzle for each disturbance and

their corresponding velocities V at 3 cm from the opening. These values are strictly used to plot the evolution of the backflow factor K(%) in section 4.

Counter-current internal free jet		Internal transverse wall jet		External transverse wall jet	
V_0 (m/s)	V (m/s)	V_0 (m/s)	V (m/s)	V_0 (m/s)	V (m/s)
1.81	0.52	6.71	1.85	5.8	1.66
3.23	0.94	8.35	2.55	9.83	2.52
5.51	1.63	10.51	3	14.1	3.8
7.72	2.12	13.29	3.55	17.44	4.6
9.45	2.84	15.47	4.05	20.08	5.75
11.55	3.2	17.87	4.6	23.98	6.85
14.13	3.9	21.20	5.35	25.79	7.5

Table 1 Velocities V_0 at the outlet of the nozzle and V at 3 cm from the opening for each disturbance.

3.1. Visualization of the backflow

External transverse wall jet

Considering the case of an interaction between the confinement air flow and an external transverse turbulent jet flow, two experimental campaigns have been conducted. The injection velocity of the perturbation jet from the nozzle was fixed to $V_0 = 25.5$ m/s outside the enclosure. Two distances between the opening center and the injection nozzle were chosen: 45 cm and 24 cm. In this way, the turbulent jet reaches transversally the opening with two velocities, V = 5 m/s and V = 6.8 m/s respectively. These two values were measured at the opening central point by a hot-wire anemometer without any extraction flowrate in the enclosure. Fig. 8 shows the behavior of the gas tracer at the opening due to the interaction between the confinement inflow and the external transverse turbulent jet for each flow velocity, on a vertical plane at the opening outside the enclosure. The cropped visualization field is a $(40 \times 40)\ cm^2$ square. According to the corresponding flow visualization, leakage is detected in both cases. While comparing Fig. 8(a) and Fig. 8(b), we found that more vigorous vortices are observed in the case where the injection nozzle is located closer to the opening Fig. 8(b), hence when V is higher.

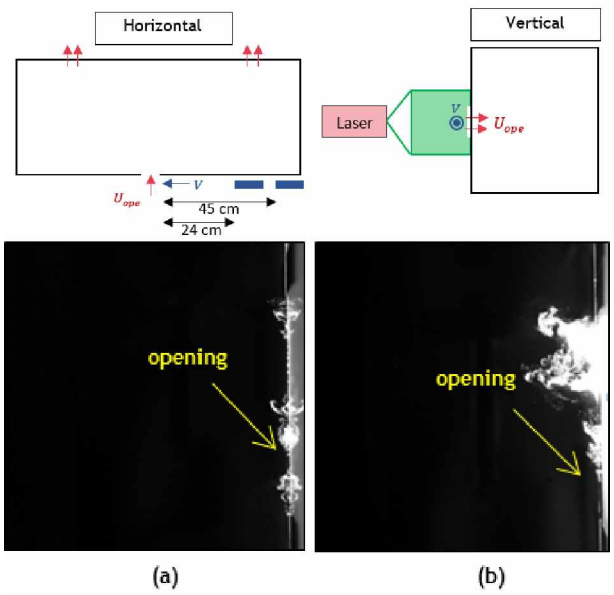

Figure 8 Top: Schemes of the external wall jet perturbation in the horizontal and vertical planes. Bottom: Laser tomography visualization of tracer leakage in the vertical plane outside the enclosure in the case of external transverse jet of velocity: (a) V = 5 m/s , (b) V = 6.8 m/s for U_{ope} = 1 m/s.

Internal counter-current perturbation

In this case, we show the interaction between the initial airflow at the opening and four configurations of internal counter-current turbulent jets corresponding to three velocities at the nozzle exit that are V_0 = 3 m/s, 6 m/s, 8.4 m/s and 11.7 m/s respectively. The counter-current internal jet disturbance was generated from the nozzle facing the opening inside the enclosure as described in section 2.2. Fig. 9 illustrates instantaneous laser tomographic visualizations of the flow tracer in the median vertical plane of the opening. Note that the inside of the enclosure is at the left of each figure, while the outside of the enclosure is at the right of each figure. The visualization zone corresponds to a surface of $(30 \times 30)\ cm^2$.

We note that for a turbulent jet of 3 m/s velocity at the nozzle exit, as shown in Fig. 9(a), there is no leakage of the tracer to the outside of the enclosure. The external air continues to enter the enclosure through the opening resulting in a small region free

of tracer inside the enclosure near the opening. The dynamic confinement succeeds to prevent gas backflow. While applying a jet of a velocity of 6 m/s as shown in Fig. 9(b), the leakage of the tracer to the outside of the enclosure starts to occur: we observe vortex shedding close to the opening. This backflow phenomenon appears in the form of random puffs with resumption of majority of the tracer to the inside of the enclosure. The dynamic confinement efficiency starts to break-up. For a higher velocity of 8.4 m/s as shown in Fig. 9(c), there is a continuous leakage of the tracer to the outside of the enclosure with strong vortex shedding at the opening. While increasing the velocity to 11.7 m/s as shown in Fig. 9(d), the continuous dispersion of the tracer to the outside of the enclosure is enhanced. The dynamic confinement fails to protect the environment outside the enclosure in these cases ((c) and (d)).

3.2. Flow velocity measurements

Internal counter-current perturbation

PIV measurements presented here show the interaction between the confinement inflow and an internal counter-current turbulent jet, at the vertical median plane of the opening inside the enclosure. Four configurations of nozzle jet velocities V_0 (3.2 m/s, 6 m/s, 8.4 m/s and 11.7 m/s) were studied. The time between two laser pulses for each configuration is set to $\Delta t = 1\ ms$. The inter-correlation algorithm applies an adaptive PIV method with a grid step size of 64 × 64 pixels, a minimum interrogation area size of 64 × 64 pixels and a maximum interrogation area size of 128 × 128 pixels. A statistical average is carried out on 400 images for each configuration of the flow and their corresponding mean velocity fields in the vertical median plane of the opening are shown in Fig. 10.

For a counter-current turbulent jet velocity $V_0 = 3.2$ m/s (Fig. 10(a)), the mean flow inside and outside the enclosure near the opening is oriented horizontally towards the inside of the enclosure. The velocity near the opening inside the enclosure has a value close

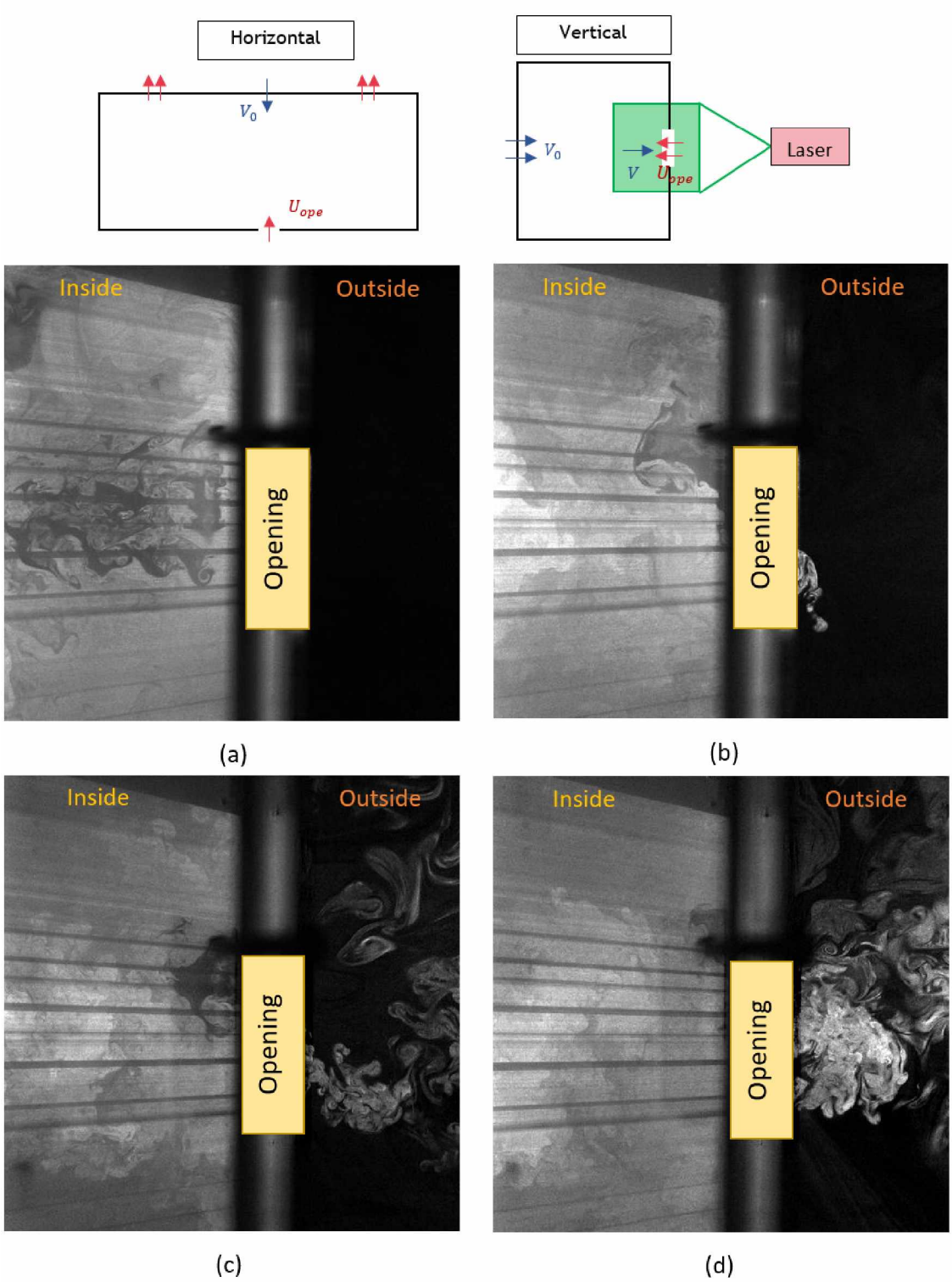

Figure 9 Top: Schemes of the internal counter-current disturbance in the horizontal and vertical planes. Bottom: Laser tomography visualization of tracer leakage at the vertical median plane at the opening in the case of an internal counter-current jet velocity: (a) $V_0 = 3.2$ m/s , (b) $V_0 = 6$ m/s, (c) $V_0 = 8.4$ m/s and (d) $V_0 = 11.7$ m/s for $U_{ope} = 1$ m/s.

to 0.5 m/s and outside the enclosure about 0.1 m/s. In this case, there was no backflow outside the enclosure as already observed in the corresponding visualization fields in Fig. 9(a). For a counter-current turbulent jet velocity $V_0 = 6$ m/s as shown in Fig. 10(b), the direction of the mean flow near the opening inside the enclosure is horizontally towards the outside of the enclosure with mean velocity about 0.6 m/s. For the region outside the enclosure, the direction of the mean flow near the opening is towards the inside of the enclosure and is about 0.07 m/s. Here, the corresponding visualization fields indicate the occurrence of weak tracer backflow (Fig. 9(b)), but the majority of the tracer is taken back to the inside of the enclosure. For $V_0 = 8.4$ m/s (Fig. 10(c)), the mean flow direction inside the enclosure is towards the outside of the enclosure and of the order of 0.9 m/s. For the region outside the enclosure, the mean flow is towards the outside the enclosure and has a mean velocity of 0.12 m/s. In this case, the counter-current turbulent jet is strong enough to overcome the dynamic air inflow and leads the tracer to the outside of the enclosure. As we increase the counter-current turbulent jet velocity V_0 to 11.7 m/s as shown in Fig. 10(d), the mean velocity field is towards the outside of the enclosure and is of the order of 1 m/s inside the enclosure and 0.3 m/s outside the enclosure. There is a continuous dispersion of tracer outside the enclosure.

4. Comments on backflow measurements

In the following, we comment on pollutant dispersion in terms of the backflow factor evolution. However, we assumed in our study that C_{air} is negligible compared to $\overline{C_{in_{eq}}}$ (typically $C_{air}/\overline{C_{in_{eq}}}$ is less than 1%) and that the flowrate of the injected tracer q_0 is negligible compared to the extraction flowrate of the enclosure Q_{ext} (typically q_0/Q_{ext} is less than 0.1%). Based on these assumptions, the transfer coefficient k (s/m^3) can be directly calculated from our backflow factor K using Eq. 8.

$$kQ_{ext} = K \tag{8}$$

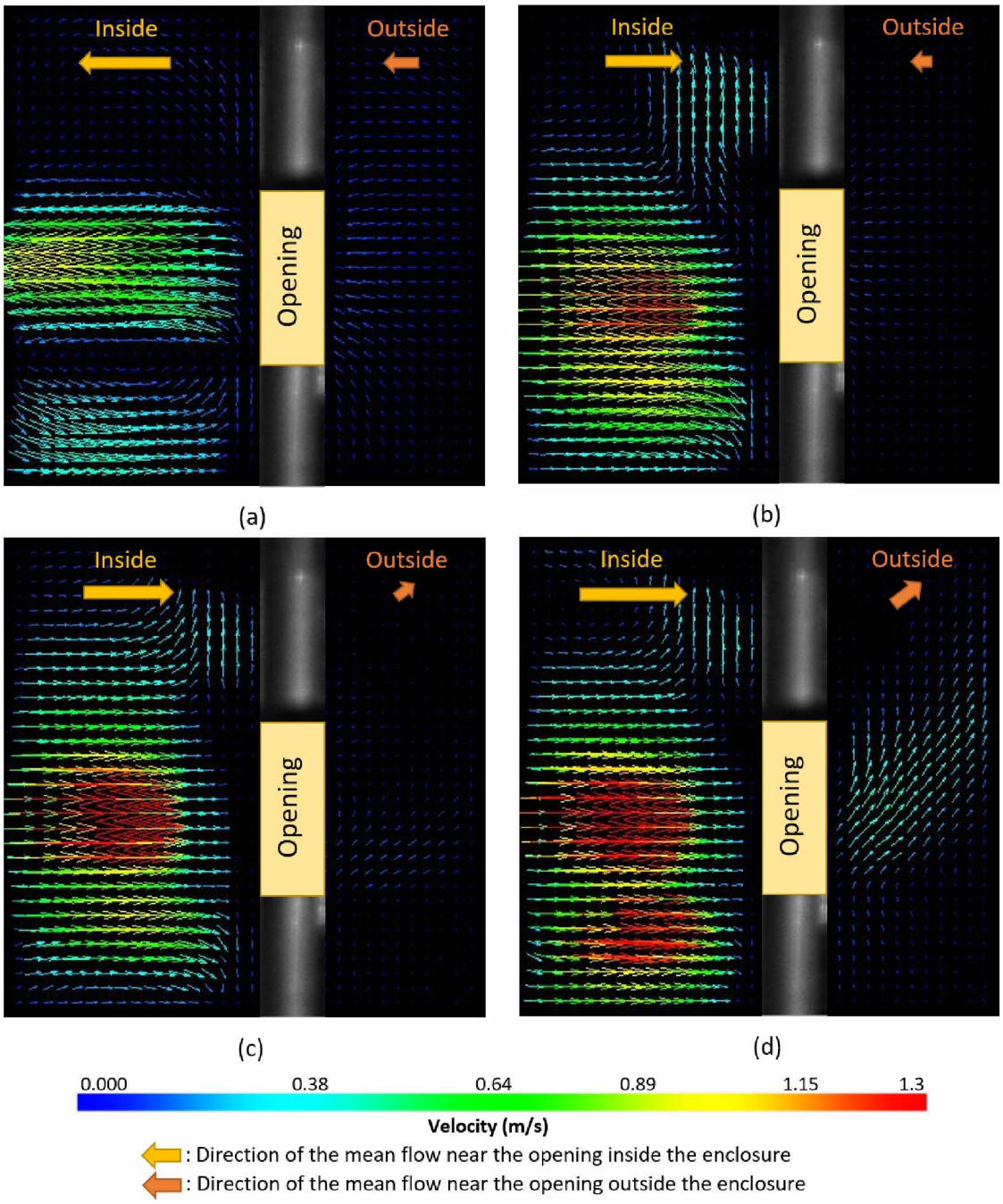

Figure 10 Time-averaged velocity fields in the vertical median plane of the opening inside and outside the enclosure representing the interaction between the inflow and an internal counter-current disturbance jet. Velocity at the nozzle outlet: (a) $V_0 = 3.2$ m/s , (b) $V_0 = 6$ m/s, (c) $V_0 = 8.4$ m/s and (d) $V_0 = 11.7$ m/s for $U_{ope} = 1$ m/s.

The evolution of the backflow factor K (%) according to V/U_{ope} has been studied for three different configurations of the disturbance jet: internal counter-current free jet, internal or external transverse wall jet. Three flowrates through the opening, corresponding to flow velocities U_{ope} equal to 0.5 m/s, 1 m/s and 1.5 m/s, have been tested for a range of disturbing velocities at the opening V ranging from 1.3 m/s to 9 m/s depending on the direction of disturbance. The repeatability of the measurements has been verified: each measurement point of the backflow evolution was systematically obtained from an average over two repetitions. The reproducibility of the results was also verified over different days during which the experimental conditions varied slightly (variation of the ambient temperature, recalibration and control of the drift of mass spectrometers, restart of all measuring devices, repositioning of the measuring points, etc.). The detection threshold of the backflow is defined when a minimum helium concentration of air / helium mixture detected at the opening, outside the enclosure, is $\overline{C_{out_{eq}}} - C_{air} = 1$ ppm ($\pm$ 50%). The minimum backflow factor which can be measured is of the order of $K = 0.1\%$ ($\pm$ 50%).

Counter-current internal free jet disturbance

The evolution of the backflow factor K (%) as a function of V/U_{ope} is studied in the case of the disturbance produced by a counter-current internal free jet for three inflows at the opening: $U_{ope} = 0.51$ m/s ($\pm$ 7.72%), $U_{ope} = 1.04$ m/s ($\pm$ 18.14%) and $U_{ope} = 1.56$ m/s ($\pm$ 5.4%), for a range of disturbing flowrates at the opening corresponding to V between 1.5 m/s and 4 m/s.

The evolution of the backflow factor K (%) as a function of the dimensionless parameter V/U_{ope} is presented in Fig. 11 for the different flowrates entering at the opening. It

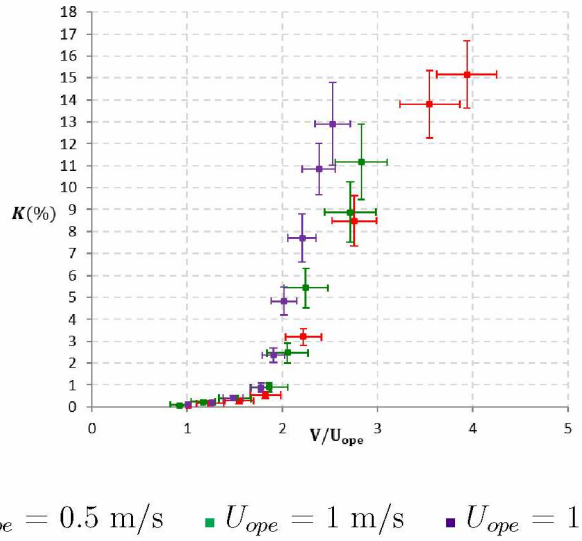

Figure 11 Evolution of the backflow factor K (%) as a function of V/U_{ope} for an internal counter-current free jet disturbance.

can be observed that regardless of the magnitude of confinement velocity at the opening, the backflow phenomenon occurs for a perturbation velocity of the same order as U_{ope} corresponding to the ratio $V/U_{ope} \approx 1$. We can also note that the three evolution curves are overlapped for $V/U_{ope} \leq 1.8 \pm 0.2$. Beyond this value, for $2 \leq V/U_{ope} \leq 4$, the measuring points are progressively scattered.

For the three cases, the part of the graph corresponding to $V/U_{ope} \leq 2$ clearly shows that the occurrence of the backflow phenomenon is determined by a critical threshold V/U_{ope}, within uncertainties, regardless of the flowrate of the dynamic confinement imposed on the opening. Note that in this part of the evolution, the backflow factor does not exceed 1%.

Internal transverse wall jet disturbance

In Fig. 12, the evolution of the backflow factor K (%) as a function of the dimensionless aeraulic parameter V/U_{ope} in the case of a transverse internal wall jet disturbance is

presented for three inflows at the opening: $U_{ope} = 0.52$ m/s ($\pm$ 5.4%), $U_{ope} = 1.03$ m/s ($\pm$ 6.4%) and $U_{ope} = 1.52$ m/s ($\pm$ 5.58%), for a range of disturbance velocities V at the opening ranging from 1.3 m/s to 8 m/s.

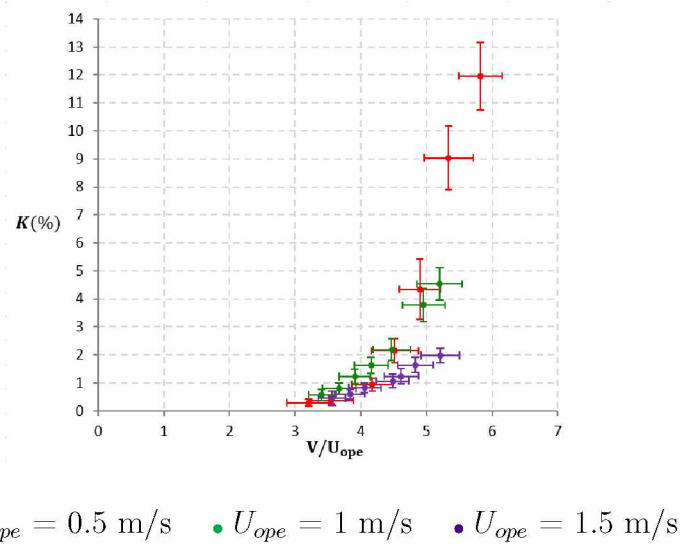

Figure 12 Evolution of the backflow factor K (%) as a function of V/U_{ope} for the case of internal transverse wall jet disturbance.

The onset of backflow is observed for the three flowrates at $V/U_{ope} = 3.5 \pm 0.2$ with a good overlap beyond that point. Under these flow conditions, the occurrence of leakage at the opening and dispersion of pollutant are adequately rationalized by V/U_{ope} for $V/U_{ope} \leq 4$. Beyond this value, the curves are no longer overlapping and there are non-negligible differences in the backflow intensity. For example, for the same ratio $V/U_{ope} = 5.2$, the backflow factor is more important when the flowrate is smaller which means that measured quantity of pollutant outside the enclosure is more effective.

External transverse wall jet disturbance

The evolution of the backflow factor K (%) as a function of V/U_{ope} is studied for the case of the transverse external wall jet for three inflows at the opening corresponding to

$U_{ope} = 0.49$ m/s ($\pm$ 8.4%), $U_{ope} = 1.03$ m/s ($\pm$ 5.3%) and $U_{ope} = 1.55$ m/s ($\pm$ 8.3%). The range of disturbance velocities at opening V we tested is between 1.6 m/s and 9 m/s and corresponds to results of fig. 13.

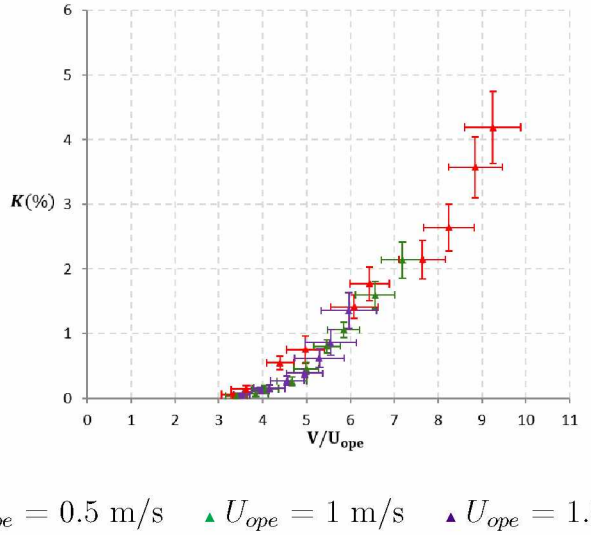

▲ $U_{ope} = 0.5$ m/s ▲ $U_{ope} = 1$ m/s ▲ $U_{ope} = 1.5$ m/s

Figure 13 Evolution of the backflow factor K (%) as a function of V/U_{ope} for transverse external wall jet disturbance.

We can clearly observe that the three sets of data for the backflow factor K (%) are overlapped (within uncertainties of experimental measurements) for the range of studied experimental conditions. The onset of the backflow phenomenon is around $V/U_{ope} = 3.5 \pm 0.25$. We can conclude that the effect of aeraulic opening conditions on the backflow factor is adequately characterized by the dimensionless parameter V/U_{ope} over the whole range of V/U_{ope} we studied.

As we can expect, the external disturbance jet presents much less backflow compared to the internal disturbance configuration. Indeed, in the case of internal jets, the disturbance comes from a closed aeraulic network connected to the enclosure filled with helium during the test. At equilibrium, the jet produced by this aeraulic network is charged with helium, which implies that the tracer concentration in the internal zone near the opening

remains homogeneous over the duration of the test. In the case of an external perturbation the jet is made of to ambient air. Therefore, the external area close to the opening is continuously swept with fresh ambient air free of helium which reduces the leakage of pollutant compared to internal perturbations.

5. Conclusion

The transfer of gaseous pollutant outside a ventilated enclosure through existing or accidental openings is commonly referred to as backflow. This phenomenon is more likely to occur for enclosures under low pressure compared to their external environment, such as maintenance or dismantling airlocks implemented in nuclear facilities. Because very few investigations were carried out on characterizing flow inversion phenomena at rectangular slits in depressurized enclosures, the approach we adopted was to reproduce the phenomenon under different controlled configurations and to measure the intensity of gas tracer as a surrogate for pollutant dispersion. To this aim, we performed experiments on an experimental enclosure to which an aeraulic disturbance system was added to generate internal or external disturbances. It has been observed that an additional turbulent flow (typically a jet) either inside the enclosure or outside can cause leakage at the opening.

Visualization techniques offer the opportunity to detect the leakage of gas tracer in the presence of turbulent jets, and visualize the inversion due to unsteady vortices near the opening. The PIV technique provides information on local flow structure and magnitude of the velocity of the turbulent flow near the opening in the presence of the disturbance jet. It also gives quantitative information on the velocity V of the perturbation flow near the opening. We are aiming at determining the conditions that are prone to generate backflow for different types of disturbance. The observations help to conclude that two conditions must be met in order to yield significant backflow phenomenon at openings:

the presence of specific aeraulic conditions as well as the presence of continuous supply of tracer in the vicinity of the internal side of the opening.

Gas tracing technique was applied to quantify the backflow phenomenon for different scenarios of external or internal disturbance turbulent jet. The evolution of the backflow factor K as a function of the dimensionless aeraulic parameter V/U_{ope} for different dynamic confinement flowrates through the opening U_{ope} showed that this dimensionless velocity was relevant to characterize the effect of the aeraulic conditions on the onset of backflow. This was done for all three types of turbulent jet disturbances we tested.

The ISO standards[1, 2] recommendation relies on a constant inflow velocity at the opening whatever the operating conditions, depending only on the nature of the pollutant species. Simultaneously, the ISO standards indicate that each scenario must be studied specifically. Our study has shown that the constant inflow velocity at the opening recommendation does not provide a conservative prediction of gaseous pollutant backflow phenomenon. Indeed, depending on the direction of flow perturbation, the critical conditions for the onset of pollutant dispersion are characterized by a specific value of V/U_{ope}. This means that for a fixed value of the confinement velocity U_{ope}, backflow of pollutant will occur if the perturbation velocity is large enough. This typical value is $V/U_{ope} = 1$ for a counter-current jet and $V/U_{ope} = 3.5$ for transverse flows. Above this critical value, the amount of backflowed gas depends also on the type of perturbation, the counter-current jet being the most dangerous. Comparing transverse jet configurations showed that internal perturbations are more prone to generate outward dispersion of tracer gas. Measurements concerning the external jet have resulted in lower intensity of pollutant dispersion.

The perspectives of this work are to study the backflow phenomenon of a particulate

pollutant, as well as to test the backflow of pollutants through a felixibile wall in order to predict and prevent them on on a real dismantling site. Simultaneously, we aim to test the ability of CFD simulations to reproduce the backflow phenomenon through openings. These works are currently in progress.

Acknowledgements

The present work was equally supported by IRSN and EDF in collaboration with IMFT in the context of nuclear safety of maintenance and dismantling sites. The authors would like to thank Luc Lafanechere, Marjorie Jacquelin and Audrey Amphoux for their special assistance and insightful comments. The contribution of Laurent Ricciardi from IRSN is gratefully acknowledged, particularly for fruitful discussions. Nadia Liatimi from IRSN is also acknowledged for her technical support.

Nomenclature

Variables

C	Tracer concentration	ppm
$\overline{C}$	Mean concentration	ppm
k	Transfer coefficient	(s/m^3)
K	Backflow factor	%
P	Pressure	Pa
P_{atm}	Atmospheric pressure	Pa
q	Flowrate of tracer	$m^3.h^{-1}$
Q	Extraction flowrate	$m^3.h^{-1}$
S	Aera of the opening	m^2
U_{ope}	Velocity at the opening	m/s
U_r	Relative uncertainty	%
V	Disturbance velocity at the opening	m/s
V_0	Disturbance velocity at the nozzle	m/s

Abbreviations

2D	Two-dimensional
CCD	Charge Coupled Device
ISO	International organization for standardization
LDV	Laser doppler velocimetry
PIV	Particle image velocimetry
PMMA	Poly-methyl methacrylate

Subscripts

0	relative to the origin
ext	relative to the extraction
in	relative to inside the enclosure
eq	relative to the equilibrium
ope	relative to the opening
out	relative to outside the enclosure

References

[1] ISO 17873. Nuclear facilities — Criteria for the design and operation of ventilation systems for nuclear installations other than nuclear reactors, 2004.

[2] ISO 16647. Nuclear facilities — Criteria for design and operation of confinement systems for nuclear worksite and for nuclear installations under decommissioning, 2008.

[3] A. Valkeapaa and H. Anttonen. Draught caused by large doorways in industrial premises. Int. J. Vent. 2004;3(1):41-51.

[4] L. Wang and Z. Zhong. An approach to determine infiltration characteristics of building entrance equipped with air curtains. Energy Build. 2014; 75:312-320.

[5] S. Goubran, D. Qi, W.F. Saleh, L. Wang, and R. Zmeureanu. Experimental study on the flow characteristics of air curtains at building entrances. Build. Environ. 2016; 105:225-235.

[6] A.M. Foster, R. Swain, M.J. and Barrett, P.D. Agaro, and S.J. James. Effectiveness and optimum jet velocity for a plane jet air curtain used to restrict cold room infiltration. Int. J. Refrigeration. 2006; 29:692-699.

[7] M. van Belleghem, G. Verhaeghe, C. T'Joen, H. Huisseune, P. de Jaeger, and M. de Paepe. Heat transfer through vertically downward-blowing single-jet air curtains for cold rooms. Heat Transf.

Eng. 2012; 33:1196-1206.

[8] P. Kalliomaki, P. Saarinen, J.W.-T. Tang, and H. Koskela. Airow patterns through single hinged and sliding doors in hospital isolation rooms. Int. J. Vent. 2015; 14:111-126.

[9] O. Rouaud. Etudes numeriques et experimentales de dispositifs de protection contre la contamination aeroportee dans les industries alimentaires. Phd thesis. Universite de Nantes, ENITIAA, Nantes, 2002.

[10] M. Havet, O. Rouaud, and C. Solliec. Experimental investigations of an air curtain device subjected to external perturbations. Int. J. Heat Fluid Flow. 2003; 24:928-930.

[11] S.C. Hu, Y.K. Chuah, and M.C. Yen. Design and evaluation of a minienvironment for semiconductor manufacture processes. Building and Environment. 2002; 37:201-208.

[12] C.S. Hayden II, O.E. Johnston, R.T. Hughes, and P.A. Jensen. Air volume migration from negative pressure isolation rooms during entry/exit. Appl. Occup. Environ. Hyg. 1998; 13:518-527.

[13] P. Kalliomaki, P. Saarinen, J.W.-T. Tang, and H. Koskela. Airflow patterns through single hinged and sliding doors in hospital isolation rooms - Effect of ventilation, flow differential and passage. Build. Environ. 2016; 107:154-168.

[14] L. Chang, S. Tu, W. Ye, and X. Zhang. Dynamic simulation of containment inleakage produced by human walking into control room. Int. J. Heat MassTransf. 2017; 113:1179-1188.

[15] C. Chen, B. Zhao, X. Yang, and Y. Li. Role of two-way airflow owing to temperature difference in severe acute respiratory syndrome transmission: revisiting the largest nosocomial severe acute respiratory syndrome outbreak in hong kong. J. R. Soc. Interface. 2010; 8:699-710.

[16] J. Hang, Y. Li, W.H. Ching, R. Wei, J.and Jin, L. Liu, and X. Xie. Potential airborne transmission between two isolation cubicles through a shared anteroom. Build. Environ. 2015; 89:264-278.

[17] C. Prevost and J. Lacan. Etude de l'effcacite de confinement d'une boite a gants en situations accidentelles de fonctionnement. CFA Conference, Paris, 2003.

[18] C. Prevost, L. Bouilloux, and J. Lacan. Etude de l'effcacite de confinement assure par une boite a gants en situations accidentelles de fonctionnement. SFRP Conference, Nantes. 2005.

[19] X. Cao, J. Liu, N. Jiang, and Chen Q. Particle image velocimetry measurement of indoor airflow field: A review of the technologies and applications. Energy and Buildings. 2014; 69:367-380.

[20] V. Cesard, E. Belut, C. Prevost, A. Taniere and N. Rimbert. Assessing the Containment Efficiency of a Microbiological Safety Cabinet During the Simultaneous Generation of a Nanoaerosol and a Tracer Gas. Ann. Occup. Hyg. 2013; 57:345–359.

[21] D. Song, J. Lee, S. Ha S. Huh. Assessment of control room habitability and unfiltered air inleakage test of the OPR 1000 NPP. J. Nucl. Sci. Technol. 2015; 52:905-911.

[22] Y. Iwai, T. Hayashi, T. Yamanishi, K. Kobayashi M. Nishi. Simulation of Tritium Behavior after Intended Tritium Release in Ventilated Room. J. Nucl. Sci. Technol. 2001; 38:63-75.